Invertebrate Biology

Invertebrate Biology 133(2): 188–199.

DOI: 10.1111/ivb.12054

Properties, morphogenesis, and effect of acidification on spines of the cidaroid sea urchin *Phyllacanthus imperialis*

Aurélie Dery,[1,a] Virginie Guibourt,[1] Ana I. Catarino,[1] Philippe Compère,[2] and Philippe Dubois[1]

[1] Laboratoire de Biologie Marine, Université Libre de Bruxelles, Brussels B-1050, Belgium
[2] Laboratoire de Morphologie évolutive et fonctionnelle, Biologie, Ecologie et Evolution (BEE) et Cellule d'Appui Technologique en Microscopie, Université de Liège, Liège 4000, Belgium

Abstract. Cidaroid sea urchins are the sister clade to all other extant echinoids and have numerous unique features, including unusual primary spines. These lack an epidermis when mature, exposing their high-magnesium calcite skeleton to seawater and allowing the settlement of numerous epibionts. Cidaroid spines are made of an inner core of classical monocrystalline skeleton and an outer layer of polycrystalline magnesium calcite. Interestingly, cidaroids survived the Permian-Triassic crisis, which was characterized by severe acidification of the ocean. Currently, numerous members of this group inhabit the deep ocean, below the saturation horizon for their magnesium calcite skeleton. This suggests that members of this taxon may have characteristics that may allow them to resist ongoing ocean acidification linked to global change. We compared the effect of acidified seawater (pH 7.2, 7.6, or 8.2) on mature spines with a fully developed cortex to that on young, growing spines, in which only the stereom core was developed. The cortex of mature spines was much more resistant to etching than the stereom of young spines. We then examined the properties of the cortex that might be responsible for its resistance compared to the underlying stereomic layers, namely morphology, intramineral organic material, magnesium concentration, intrinsic solubility of the mineral, and density. Our results indicate that the acidification resistance of the cortex is probably due to its lower magnesium concentration and higher density, the latter reducing the amount of surface area in contact with acidified seawater. The biofilm and epibionts covering the cortex of mature spines may also reduce its exposure to seawater.

Additional key words: echinoderm, global change, skeleton, solubility

Introduction

Since the beginning of the industrial revolution, atmospheric CO_2 concentration has been rising at a rate 100 times higher than ever recorded over geological history (Zeebe 2012). About a third of this CO_2 has been absorbed by the ocean, leading to reductions in carbonate ion concentration, seawater pH, and the saturation state of calcium carbonates, a set of phenomena known as ocean acidification (Feely et al. 2004; Orr et al. 2005). As a consequence, surface seawater pH is already 0.1 units lower than preindustrial values, and an additional decrease of 0.4 units by the end of the 21st century is predicted (Pelejero et al. 2010). Subsequently, the saturation horizons of calcium carbonates will become more shallow, especially at the poles. This effect will be especially dramatic for the most soluble forms, aragonite and high magnesium calcite (Feely et al. 2009).

Acidification will very probably have drastic impacts on marine fauna, especially for organisms that have a weak acid-base regulation capacity, such as echinoderms (Pörtner et al. 2004; Melzner et al. 2009). Echinoderms are considered as particularly at risk as they have a well-developed high-magnesium calcite endoskeleton whose precursor is a transient amorphous calcium carbonate (ACC) phase, a form of $CaCO_3$ 30 times more soluble than calcite (Politi et al. 2004). However, their skeleton is produced in a tightly closed space delimited by skeletogenic cells, where ionic conditions are controlled by different transporters (Dubois & Chen 1989; Stumpp et al.

[a]Author for correspondence.
E-mail: auredery@gmail.com

2012). Furthermore, this skeleton is produced either in the mesoderm (larvae) or in the dermis (adults), and is almost never directly exposed to seawater. Indeed, larvae and adult echinoderms are able to calcify and to maintain their skeleton at a saturation state below 1, both in experimental conditions and in the field (David et al. 2005; Dupont et al. 2010; Byrne 2011). The influence of acidification on the echinoderm skeleton is thus mainly viewed as an indirect one, most likely due to weak acid-base regulation or to metabolic depression (Pörtner 2008; Hofmann & Todgham 2010).

Cidaroid sea urchins are the sister clade to all other echinoids (the latter being called "euechinoids") (Kroh & Smith 2010). They differ from euechinoids in several respects. In particular, their mature primary spines are devoid of epidermis, so that the skeleton is in direct contact with seawater. These spines are made of several layers (Märkel et al. 1971; Grossmann & Nebelsick 2013). The central zone (the medulla) and the median layer are made of a network of trabeculae (the stereom), are monocrystalline (Märkel et al. 1971), and are similar to the homologous layers of euechinoid spines. The pores between the trabeculae are occupied by a connective tissue, the stroma, composed of an extracellular matrix and various cell types (Märkel & Röser 1983a). In cidaroids, these layers are surrounded by an outer layer, the cortex (Fig. 1). The latter is polycrystalline and is composed of dense mineral crossed by channels in which bundles of fibers and connective cells occur (Märkel et al. 1971; Märkel & Röser 1983a). The cidaroid primary spine skeleton is built by so called sclerocytes, in the dermis, separated from seawater by an epidermis (Märkel & Röser 1983a). Once the spine is fully developed (including the cortex), the epidermis disappears and the cortex comes into contact with seawater (Märkel & Röser 1983a). As a consequence, it is rapidly colonized by epibionts including perforating taxa (David et al. 2009). Both the cortex and the underlying layers are made of high-magnesium calcite and include intramineral organic material (Märkel et al. 1971). Although the morphology of mature spines has been well documented, morphogenesis of the spine skeleton, especially the cortex, is poorly understood (Borig 1933; Märkel et al. 1971; Grossmann & Nebelsick 2013).

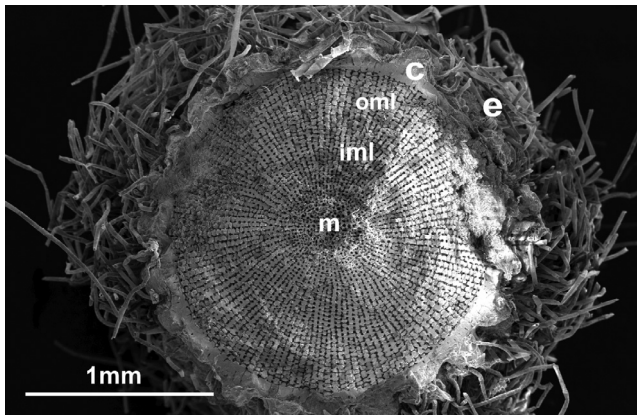

Fig. 1. Scanning electron micrograph of a cross section of a mature primary spine of the cidaroid sea urchin *Phyllacanthus imperialis,* prepared by conventional fixation (see Methods). c, cortex; e, epibionts; iml, inner median layer; m, medulla; oml, outer median layer.

Surprisingly, cidaroids are well-represented in the deep-sea fauna, especially in the Southern Ocean, living below the saturation horizon for aragonite (a proxy for the saturation horizon for high-magnesium calcite) (David et al. 2005). Furthermore, members of this group survived the Permian-Triassic crisis, which was characterized by severe acidification (Twitchett & Oji 2005). This suggests that features of cidaroid spines could allow them to resist dissolution in seawater that is under-saturated with respect to magnesium calcite. Here we investigated the morphogenesis and structural properties of primary spines of a cidaroid, and assess the effect of acidified seawater on cidaroid spines.

Methods

All studies were carried out on spines of the commercially available tropical cidaroid *Phyllacanthus imperialis* (Lamarck 1816). The sea urchins, all of which came from a single population in the Philippines, were purchased from the company De Jong Marinelife (the Netherlands). They were kept in an aquarium at 34.4 psu salinity, pH 8.1, and 27°C. They were fed *ad libitum* with artificial sea urchin food (Zeigler™, USA).

Microscopy of the cortex and organic matrix

Mature and young spines were collected from two individual urchins. The spines were cut into several segments of ~2 cm in length and were submitted to different treatments.

Scanning electron microscopy. Spine segments were prepared for scanning electron microscopy (SEM) in one of the following ways: (1) they were cleaned in 4% sodium hypochlorite (SH) for 10–30 min, rinsed with MilliQ water, and air-dried; (2) they were fixed in 3% glutaraldehyde in 0.1 mol L^{-1} sodium cacodylate buffer (1.55% NaCl, pH 7.8) for

1 h ("conventional fixation," CF), washed in cacodylate buffer, post-fixed in 1% osmium tetroxide in cacodylate buffer for 1 h, then washed again in cacodylate buffer; (3) they were treated with 2% (v/v) acetic acid (AA) for 10, 20, 30, or 60 min (Ameye et al. 2001), washed in cacodylate buffer, and then prepared by the CF method; (4) they were prepared by the CF method, except that 1% tetrasodium EDTA was added to the fixation solution (Dubois 1991) or (5) they were treated with 0.1 mol L^{-1} trichloracetic acid (TCA) for 10 min, rinsed in cacodylate buffer, and then prepared by the CF method (Dubois 1991).

Except for those specimens prepared using the SH method, specimens were dehydrated in a graded ethanol series and dried by the critical point method using CO_2 as transition fluid (using a Polaron critical point dryer). All specimens were mounted on aluminum stubs, coated with gold (JEOL JFC-1100E) and observed in a JEOL JSM-6100 scanning electron microscope. Images were acquired using SemAfore JEOL 3.0 1993–1997 software (J. Rimppi Oy, Finland).

Light microscopy. A mature primary spine was treated by the CF method and embedded in Epofix resin (Struers). Sections ~50 μm thick were cut using a diamond saw, mounted on histological slides, and polished with silicon carbide to a thickness of 10–20 μm. The slides were rinsed with ethanol and observed with a light microscope with polarized light to determine the mono- or polycrystalline nature of different parts of the cortex. They were then incubated under constant stirring for 5, 10, 15, 20, or 30 min at 37°C in a filtered solution of 0.5% acetic acid, 15.5% glutaraldehyde, and 1% Alcian blue (Mutvei solution: Schöne et al. 2005). The slides were rinsed, air-dried, and observed with a light microscope.

Cortex and stereom magnesium content

Three mature spines were removed from each of three individuals of *P. imperialis* (n=9). The spines were embedded in a pre-accelerated polyester resin (Polyester MI42 MIDA composites) to which was added 2% by volume of hardener (hardener MEC). The embedded spines were cut transversely into 5 mm slices with a diamond saw. The resulting sections were glued to microscope slides and polished with sandpaper of decreasing grit size. The final polishing was performed using 1 μm diamond powder in nonaqueous solution (Escil 1 PS-1MIC). The polished slice was carbon-coated in a Balzers BAF-400 rotary evaporator. Elemental energy dispersive X-ray (EDX) analysis was performed in an environmental SEM (FEI XL30 ESEM-FEG) operating at 10 kV, and at a working distance of 10 mm.

Four separate areas were defined on the surface of each spine cross section: the cortex (c), the outer median layer (oml), the inner median layer (iml), and the medulla (m) (Fig. 1). Spectra were acquired three times in each part of the nine cross-sections. Following this, three subparts were defined within the cortex: outer superior cortex (osc), outer inferior cortex (oic), and inner cortex (ic). Spectra were acquired three times in each of these areas of six cross-sections of six spines from two individuals.

Analyses were carried out on the surface of 1–10 μm^2 size mineral zones, with a normalized acquisition time of 100 s. The elemental quantitative analysis used an automatic background subtraction and a ZAF correction matrix to calculate the elemental composition in atomic percent. The composition was corrected by subtraction of the coated carbon added for the analyses. The $MgCO_3$ molecular percentage was calculated from the elemental composition in atomic percent (Moureaux et al. 2010).

Solubility and density of the cortex and stereom

One spine was sampled from each of three individuals. From each spine, the cortex was separated from the underlying stereom layers using a razor blade. Cortex and median layer/medulla samples were ground separately in an agate mortar and sieved into different grain size fractions: 250–125, 125–63, and <63 μm. The last fraction was most abundant and was used for experiments. The <63 μm powder from each of the three spines was heated for 6 h at 170°C (a technique called annealing: Walter & Morse 1984). Thereafter, 0.005 g of each sample was suspended in 35 mL of filtered 33.8 psu artificial seawater (Wiegandt). The suspension was constantly agitated at 20°C. Then, 200 μL of 0.1 mol L^{-1} HCl was added, and every 10 s for the next hour, a pH measurement was performed using a Metrohm pH-meter (826 pH mobile, Electrode Metrohm 6.0224.100) calibrated with Certi-PUR Buffer solutions (pH 4.00 and 7.00).

The skeleton density (percentage of cortex or stereom cross-sectional area occupied by mineral) was determined in nine mature spines from three individual urchins (three spines from each individual) by analysis of SEM images using ImageJ software (NIH).

Impact of acidified water on spines

Twelve young spines (covered by epidermis) and 12 mature spines (no longer covered by epidermis), taken from three urchins (four spines of each type were taken from each urchin), were held for 3 weeks in 260 mL sealed containers, each holding two spines of the same age and filled with filtered (0.22 μm) artificial seawater (hw Sea Salt Professional, Wiegandt GmbH) at one of three different pH levels. Three containers containing artificial seawater but no spines were included in the design. Salinity was 33.2±0.16 psu (n=36). Acidity of the artificial seawater was manipulated by bubbling CO_2 (Air Liquide) into some containers, to yield pH expressed on the total scale (pH_T) of 8.2 (control), 7.6, or 7.2. Four spines of each age were allocated to each pH treatment (four independent containers per treatment). The artificial seawater inside each container was renewed every 4 d and kept at a constant temperature (24.2±1.67°C, n=36) inside an incubator. The seawater electromotive force (e.m.f.) of each treatment was measured using an 827 pH Lab Metrohm pH meter with a combined glass electrode (Model 10 6.0258.010 with temperature sensor), calibrated with pH_{NIST} (National Institute of Standards and Technology, USA) buffers 4 and 7 (Merck CertiPUR®). The e.m.f. values were applied to the calculation of pH_T according to Del Valls & Dickson (1998). Salinity was measured using a conductivity meter pH/Cond 340i WTW. The total alkalinity (A_T) was measured by means of a potentiometric titration (Gran 1952). Information about the dissolved inorganic carbon (DIC), the carbon dioxide partial pressure (pCO_2), and the saturation state (Ω) of aragonite and calcite in each treatment was obtained using the software CO2SYS (Pierrot et al. 2006). The saturation state of the Mg-calcite was calculated using all the data obtained for the carbonate system, the ion stoichiometric activity coefficients (Millero 2001; Morse et al. 2006; Andersson et al. 2008), and the magnesium content measured by SEM-EDX at the level of the outer surface of the spine (the part exposed to seawater), which corresponds to rectilinear stereom in young spines and the cortex of mature ones (Table 1). The seawater calcium and magnesium concentrations were supplied by the hw Sea Salt professional information guide. The stoichiometric saturation (K'_S) was obtained using the "biogenic curve of Plummer & Mackenzie," also known as the "minimally prepared curve" (Plummer & Mackenzie 1974; Morse & Mackenzie 1990; Andersson et al. 2008). Parameters of the carbonate system in this experiment are presented in Table 2.

Table 1. Molar percentage of $MgCO_3$ in the different parts of the spine (mean±SD, n=3) and in the different subparts of the cortex (mean, n=2).

Parts of the spine	Molar percentage of $MgCO_3$
Cortex	5.1±0.16[a]
Outer superior	5.3
Outer inferior	5.1
Inner	6.1
Median layer	—
Outer	8.5±0.19[c]
Inner	8.1±0.31[c]
Medulla	5.9±0.48[b]

Means sharing the same superscript are not significantly different ($p<0.05$).

Data analysis

Density and $MgCO_3$ molar percentage in the cortex, median layer, and medulla were compared by two factor ANOVA with repeated measures on one cross factor (Doncaster & Davey 2007) (repeated fixed factor: parts or subparts; random factor: spines nested in random factor urchin). Multiple comparisons were performed by the Tukey test using the appropriate mean square error for the relevant mixed model according to Doncaster & Davey (2007). All statistical analyses were carried out with Systat9 software.

Results

Spine morphogenesis

Regions of young spine not yet covered by cortex had an inner medulla made of labyrinthic stereom and an outer layer of galleried stereom (stereom architecture according to Smith 1980).

The first cortical structures observed were microspines (*sensu* Heatfield 1971) of stereom growing on the surface of the outermost trabeculae of the median layer area (Fig. 2A). These microspines progressively increased in thickness and height due to the addition of successive lamellar layers (Fig. 2B). In some regions, the thickening was greater, giving rise to a boss (Märkel & Röser 1983a) or bumps (*sensu* David et al. 2009) (Fig. 2C,D). At this stage, areas with developed bosses had two distinct cortical regions: (1) an inner layer, which showed a conchoidal fracture similar to that of the stereom in untreated specimens, and concentric lamellae when the fracture was etched, and (2) an outer layer, which showed a much more irregular fracture (Fig. 2C,D). This

Table 2. Carbonate chemistry parameters during the experiment on the impact of acidified seawater. pH_T (total scale) and total alkalinity (A_T) were measured during the experiment and reported as means±standard deviations (n); DIC (dissolved inorganic carbon) and pCO_2 (partial pressure of CO_2) were calculated using CO2SYS and reported as means±standard deviations (same n as pH_T and A_T). The $\Omega_{Mg\text{-}calcite}$ was calculated by using all the data obtained for the carbonate system, the ion stoichiometric activity coefficients, and the magnesium content of the outer rectilinear stereom and the whole cortex (see Table 1) for, respectively, young spines and mature spines. Temperature was 24.2±1.67°C and salinity 33.2±0.16 psu (n=36).

Sample type	pH_T	A_T µmol kg^{-1}	DIC µmol kg^{-1}	pCO_2 µatm	$\Omega_{Mg\text{-}calcite}$
Control (empty vials)	8.2±0.10 (6)	1870±75.4 (6)	1514±91.2	183±50.9	—
	7.6±0.06 (6)	1920±78.2 (6)	1827±91.3	1080±199.2	—
	7.2±0.04 (6)	1897±117.4 (6)	1943±125.7	3018±404.9	—
Young spines	8.2±0.12 (12)	1863±75.3 (12)	1545±81.3	226±61.8	2.58
	7.6±0.06 (12)	1895±64.7 (12)	1823±68.3	1104±168.7	0.85
	7.2±0.07 (12)	1937±99.4 (12)	1969±116.3	2760±556.9	0.40
Mature spines	8.2±0.12 (12)	1869±81.8 (12)	1548±86.0	223±60.8	3.90
	7.6±0.08 (12)	1912±65.8 (12)	1839±72.0	1122±204.7	1.29
	7.2±0.07 (12)	1912±88.5 (12)	1948±104.9	2812±540.6	0.57

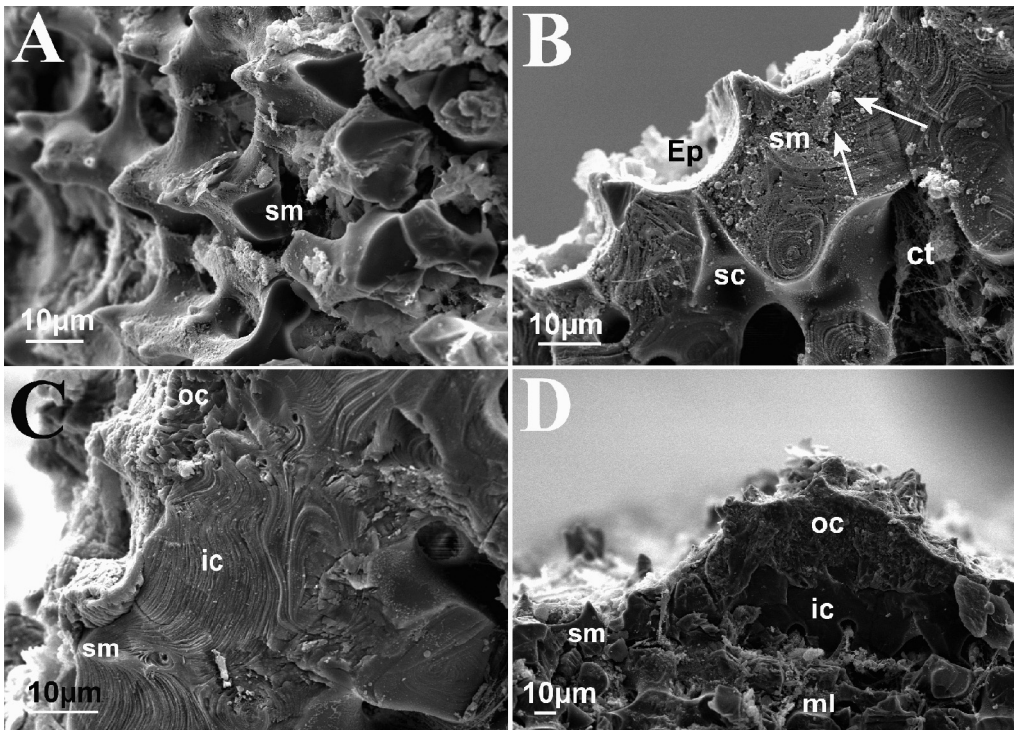

Fig. 2. Scanning electron micrographs of cross sections of a growing primary spine of *Phyllacanthus imperialis* prepared by conventional fixation (see Methods). White arrows indicate intrastereomic organic matrix. ct, connective tissue; Ep, epidermis; ic, inner cortex; ml, median layer; oc, outer cortex; sc, stromatic channels; sm, stereomic microspines.

outer layer also appeared in zones between the bosses, resulting in an additional thickening of the spine. In older spines, thorns (*sensu* Märkel & Röser 1983a) or microspines (*sensu* David et al. 2009) emerged at the level of the bosses (Fig. 3A) and eventually fused between adjacent bosses. Thereafter, they formed a network linking bosses together and surrounding the entire surface of the

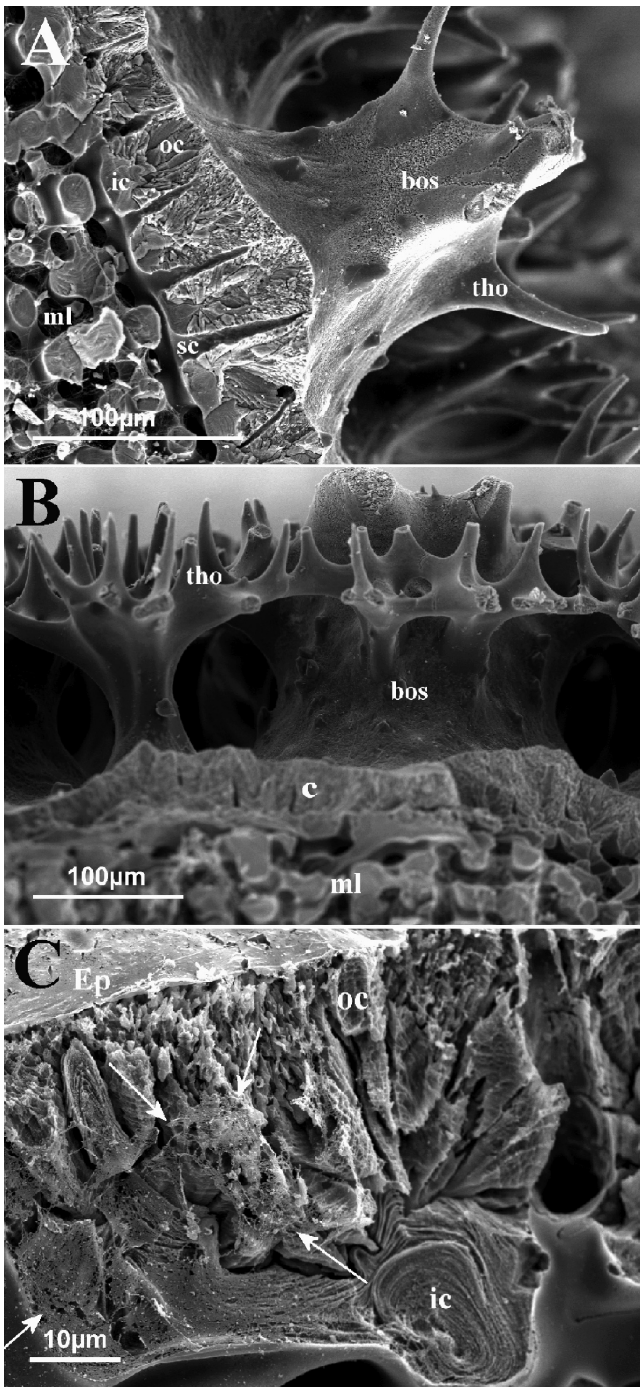

Fig. 3. Scanning electron micrographs of cross sections of a growing primary spine of *Phyllacanthus imperialis* prepared by conventional fixation (see Methods). White arrows indicate organic material. bos, boss; c, cortex; Ep, epidermis; ic, inner cortex; ml, median layer; oc, outer cortex; sc, stromatic channel; tho, thorn.

primary spine (Fig. 3B). Channels were present in the inner and outer cortex and extended through the thickness of the cortex (Fig. 3A).

The presence of organic material was highlighted by the conventional method of fixation and the treatment with acetic acid. Connective tissue containing different cell types and cell processes was found in the stereom pores and in the cortical channels (Fig. 2B). The epidermis covered the entire surface of the developing spine (Figs. 2B, 3C). Intrastereomic organic material (Fig. 3C) was revealed within the trabeculae between the mineral lamellar layers. More organic material was visible in spines with developing cortex. Nevertheless, it remained present in the cortex for the duration of its formation. No perforations except the channels were present in the developing cortex. Once the formation of the cortex was completed, the inner cortex layer had a thickness of 25–40 µm, while the outer layer could reach a thickness of 200 µm at the level of bosses.

Morphology of mature spines

In mature spines, the medulla and the median layer were similar to those described in young spines. Cross sections of trabeculae appeared as conchoidal fractures after treatment with SH (Fig. 4A) and showed concentric lamellar layers after treatment with corrosive agents (AA, TCA, EDTA) (Fig. 4B). Connective tissue was present within the pores of stereom exposed to AA, CF, TCA, and EDTA. Organic material was observed between the concentric mineral layers revealed with TCA.

The mature cortex was principally made of plain mineral with scarce channels heterogeneously distributed across its surface. Cortex treated with CF, EDTA, or SH showed a succession of mineral layers. The sections treated with SH for 30 min revealed individual crystallites and striated ridges. Channels were completely cleared of organic material and particularly visible on the sections. The sections exposed to AA were highly etched and showed clear differentiation of the inner and outer cortex (Fig. 4C,D). The inner cortex had a lamellar morphology similar to that observed in the stereom layers, while the outer cortex showed small disconnected crystallites (Fig. 4D,E). Sections treated with TCA were less etched than those submitted to AA, but otherwise showed a similar appearance. Intramineral organic material was only revealed in the cortex of segments treated with TCA (Fig. 4E). This material appeared as a network of thin fibrils in close contact with the mineral.

The Alcian blue revealed intramineral organic material in the cortex and the stereom layers. No difference in relative amount was observed (Fig. 5).

In transverse sections of spines, the medulla, the median layer and the inner cortex showed total

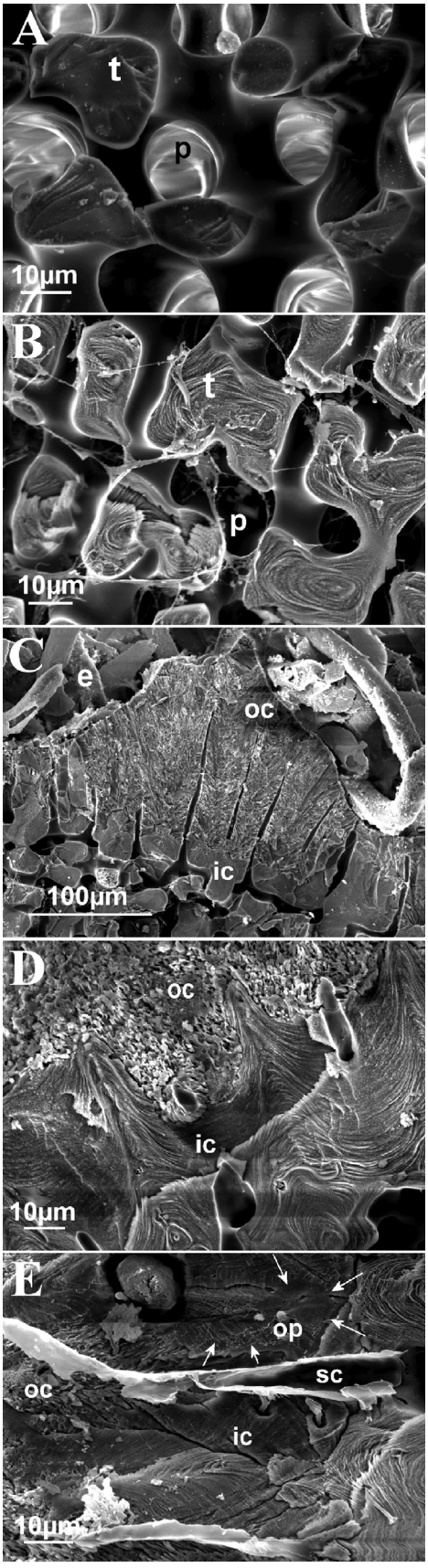

Fig. 4. Scanning electron micrographs of cross sections of mature primary spines of *Phyllacanthus imperialis*. **A.** Rectilinear stereom region. Prepared by SH. **B.** Rectilinear stereom region. Prepared by acetic acid (AA), 20 min. **C.** Cortical region. Prepared by AA, 20 min. **D.** Cortical region. Prepared by AA, 10 min. **E.** Cortical region. Prepared by trichloracetic acid, 10 min. White arrows indicate intramineral organic material. For description of preparation techniques, see Methods. e, epibionts; ic, inner cortex; oc, outer cortex; op, perforating organism; p, pore; sc, stromatic channel; t, trabeculae.

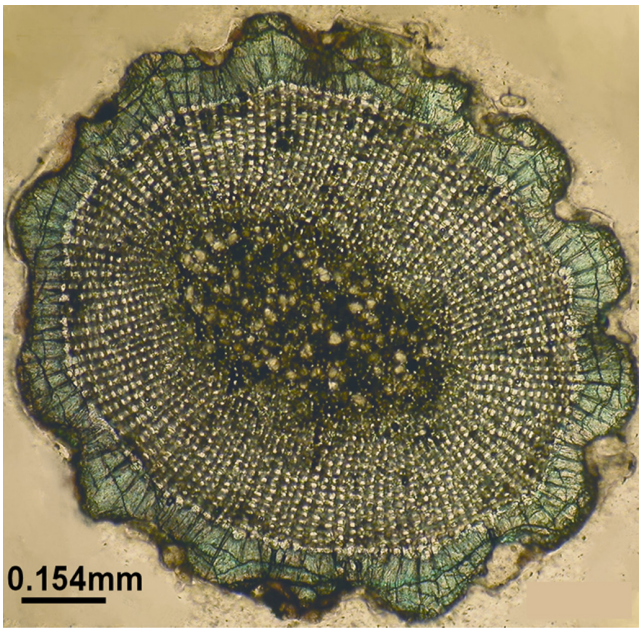

Fig. 5. Light micrograph of a cross section of a mature primary spine of *Phyllacanthus imperialis* conventionally fixed (see Methods), then colored and decalcified in a solution containing glutaraldehyde, acetic acid, and blue alcian for 15 min.

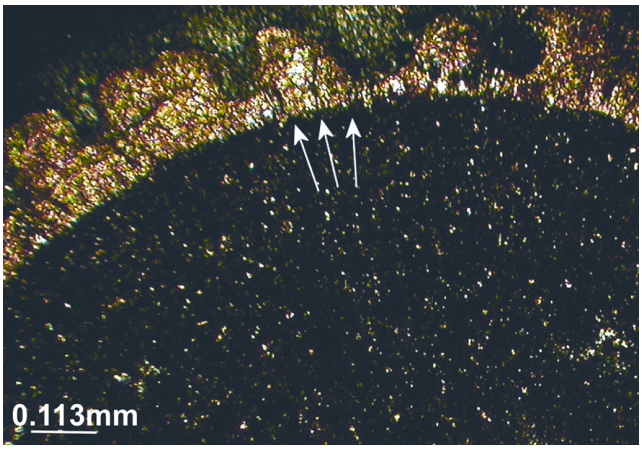

Fig. 6. Light micrograph of a cross section of a mature primary spine of *Phyllacanthus imperialis* observed with polarized light. White arrows indicate stereom microspines.

extinction between crossed nicols. In contrast, the outer cortex did not show uniform extinction (Fig. 6).

Cortex and stereom magnesium content

Spectra showed the presence of carbon, calcium, oxygen, magnesium, chlorine, sodium, and sulfur atoms in the mineral. The concentration of magnesium differed significantly according to the part of the cross section considered ($p_{Anova}<10^{-4}$; d.f.=3). The molar percentage of $MgCO_3$ was significantly lower in the cortical region than in the median layer regions ($p_{Tukey}<10^{-3}$). The two median layer regions (inner and outer) did not differ significantly from one another ($p_{Tukey}=0.235$). The medulla had a significantly lower Mg concentration than the median layer and a significantly higher Mg concentration than the cortical regions ($p_{Tukey}\leq 0.03$) (Table 1). The molar percentages also differed depending on the part of the cortex studied ($p_{Anova}=0.006$; d.f.=2), being significantly higher in the inner cortex than in the outer superior or inferior cortex ($p_{Tukey}<0.005$).

Solubility and density of the cortex and the stereom

The dissolution kinetics of the cortex and stereom layers are presented in Fig. 7. After the initial acid addition, the pH dropped suddenly and then progressively rose due to the dissolution of calcium carbonate grains of cortex or stereom. The cortex and the stereom curves were very similar (Fig. 7).

The densities (ratio between mineral area and total area in cross section) of the medulla (39±0.05%, n=3), median layer (59±0.009%, n=3), and cortex (89±0.015%, n=3) all differed from each other ($p_{Anova}<10^{-6}$; d.f.=2; $p_{Tukey}\leq 0.008$).

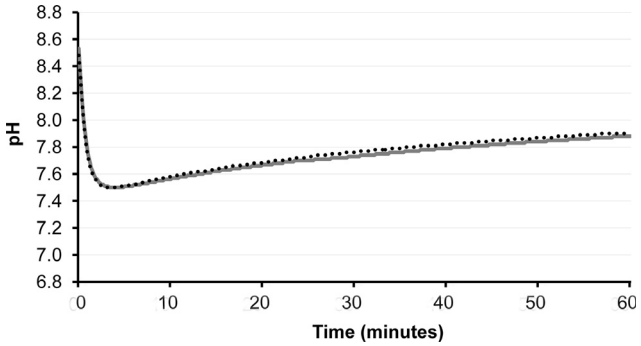

Fig. 7. Dissolution of cortex (solid line) and stereom (dotted line) magnesium calcite in artificial seawater after initial addition of HCl.

Impact of acidified water on cidaroid spines

After 3 weeks of exposure to seawater of pH 7.2, young spines were no longer covered with any protective epidermis; only patches of epidermis were visible on spines held at pH 7.6 or 8.2. Etching was obvious on the galleried stereom surface of young spines submitted to pH 7.6 or 7.2 seawater (Fig. 8A–C), while no etching was visible in young spines held at pH 8.2, despite the partly degraded epidermis. The cortex surface of mature spines showed no or very little sign of etching at pH 8.2 and 7.6, and limited etching at 7.2 (Fig. 8D–F).

Discussion

The acidification experiment showed that when submitted to a lower pH, and thus a lower Mg-calcite saturation state (Table 2), spines suffered some degree of skeletal dissolution. This phenomenon was more obvious on the surface of the galleried stereom of the younger spines than on the cortex surface of the mature spines, suggesting that the cortex is more resistant to etching than the stereom. Degradation of the epidermis and associated possible release of organic acids is not responsible for the etching of young spines, as similar degradation of the epidermis did not induce etching of the stereom at pH 8.2.

To understand the structure of the cortex and how it resist etching in the face of low saturation states, we studied its morphogenesis. This had never been described previously. Cortex formation starts with the development of microspines that grow on the surface of the median layer trabeculae. These microspines are generated and grow by successive addition of mineral layers. Once fully developed, they form the inner part of the cortex. By polarized light microscopy, they appeared to be monocrystalline, exactly like the underlying stereom. Once these microspines are formed, a second cortical layer develops heterogeneously across the surface of the spine. Some thickenings appear and make the future bosses of the mature spine. The bosses thicken gradually, developing a rounded appearance. Small thorns appear on the bosses and merge between adjacent bosses. This cortical outer layer consists of individual irregular crystallites oriented in all directions, making it polycrystalline, as described in several other cidaroid species, for example *Stylocidaris affinis* (Philippi 1845) (Borig 1933; Märkel et al. 1971). The cortex is thus composed of two layers that are distinct in both morphology and crystallography: the stereomic monocrystalline inner layer, and the thicker polycrystalline outer layer. This dual

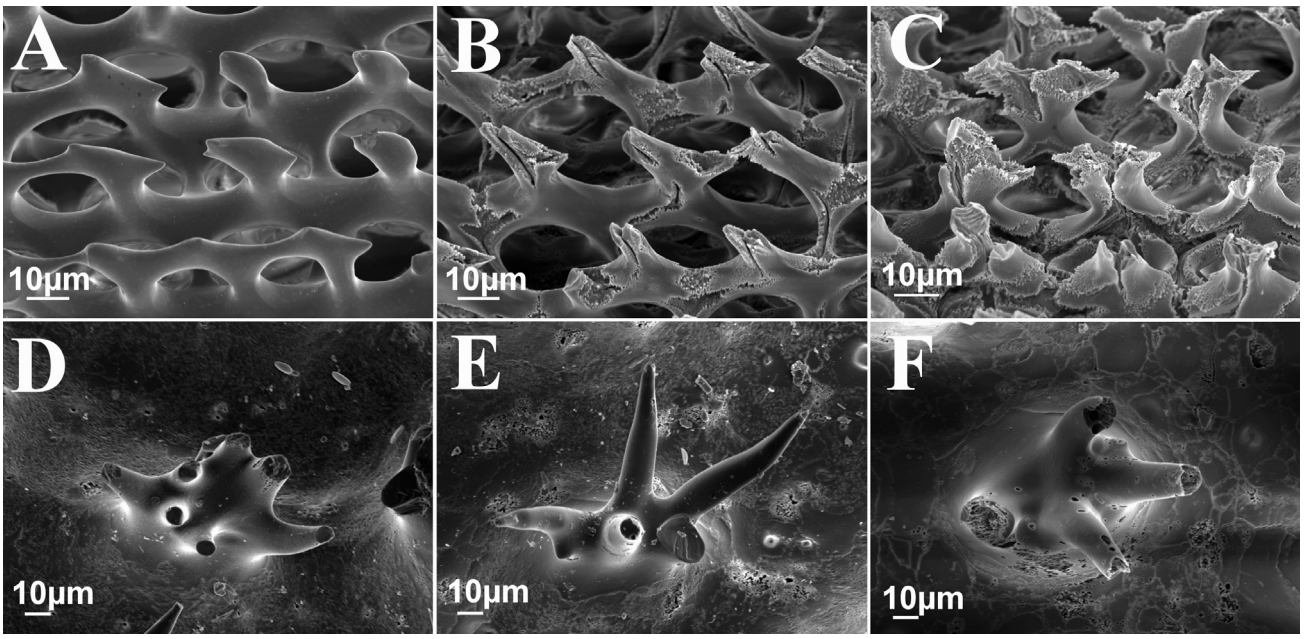

Fig. 8. Scanning electron micrographs showing lateral views of the shaft of young spines without cortex **A—C** and mature spines **D—F** of *Phyllacanthus imperialis* submitted to different pH conditions for 3 weeks. A, D: pH=8.2; B, E: pH=7.6; C, F: pH=7.2.

structure of the mature cortex was also observed in *S. affinis* (Märkel et al. 1971). The morphogenesis of the outer cortex differs from the formation of dense or imperforate stereom as described, for example, in septa of euechinoid primary spines. In the latter, these dense zones first develop by the regular branching of stereom trabeculae. The pores are secondarily filled in by crystallographically continuous calcite (Heatfield 1971; Mishor 1975). In contrast, the dense outer cortex is made by the packing of irregularly oriented microcrystals.

Various factors may influence the solubility of biogenic calcite: the presence of organic material protecting crystallites (intramineral organic material, biofilm, epibionts), magnesium concentration, or the morphology and orientation of carbonate grains (Harper 2000).

Among the different treatments applied to mature primary spines, only the treatment with TCA, which causes the precipitation of proteins, clearly demonstrated the presence of organic material within the polycrystalline mineral phase. The organic material in the cortex had the appearance of a fine network infiltrating the entire cortex outer layer. This material does not appear, however, to totally surround the crystallites, as in the case of calcite prisms of the mollusk shell (Harper 2000). Alcian blue staining also revealed the presence of organic material in the cortex and the underlying stereom (median layer and medulla). The difference in staining intensity was low or absent between the cortex and the underlying stereom. Thus, organic material is indeed present in the cortex, but in small quantities. The apparent decrease in amount of this material during morphogenesis indicates its important role in the development of the cortex, but not in subsequent protection of the cortex. This suggests that the presence of cortical organic material is not related to the resistance of the cortex to low pH conditions.

The average magnesium concentration in the cortex is 5.1 mole% $MgCO_3$. This is significantly lower than concentrations observed in the medulla (5.9 mole% $MgCO_3$) and the median layer (8.1–0.5 mole% $MgCO_3$). In addition, the magnesium concentration in the monocrystalline inner cortex is higher than that of the outer polycrystalline cortex. Similar results were obtained by Märkel et al. (1971) in the cortex of *S. affinis*, suggesting that this is a general property of the cortex and could affect the solubility of the latter. Indeed, at pH 7.6 seawater is still supersaturated relative to the cortex ($\Omega>1$) while it is undersaturated relative to the median layer (Table 2). At pH 7.2, seawater is undersaturated towards both layers. Indeed, both the cortex and median layer were etched at pH 7.2, although the former layer was much less affected than the latter. These differences in saturation state are due to differences in magnesium concentration of the exposed layers. Thus, the differential etching of the outer skeletal layer of spines (cortex or median

layer) can be linked to the magnesium concentration of the mineral. It is noteworthy that the cortex magnesium concentration of primary spines of the Antarctic cidaroid *Ctenocidaris speciosa* Mortensen 1910 is lower in specimens collected below the saturation horizon for aragonite (a proxy for the saturation horizon for magnesium calcite in deep specimens for which K_{sp} of the latter mineral cannot be calculated) (Catarino et al. 2013). However the dissolution experiment, carried out on grains of uniform size, did not reveal a marked difference in global solubility between the cortex and the underlying stereom, indicating that another factor is involved.

The density of the cortex appeared to be much higher than that of the median layer and medulla, as already reported qualitatively by several authors, starting with Mortensen (1928). This means that the surface to volume ratio of the cortex is much lower, which should slow dissolution. The high density of the cortex is explained by its morphogenesis, proceeding by successive addition of material and not by the regular branching of trabeculae occurring during stereom growth. Furthermore, calcite is a compound whose anisotropic properties vary according to crystal orientation. Calcite crystals are more sensitive to dissolution along the *c* axis (Harper 2000). As the stereom layers are monocrystalline, with the *c*-axis aligned with the long axis of the spine (as evidenced by extinction of cross sections between crossed nicols), their dissolution, once started, may proceed easily. On the contrary, the crystallites of the outer cortex have multiple orientations and are not in crystallographic continuity. Therefore, the dissolution process would be slower in the cortex, and the polycrystalline nature of the outer cortex may be adaptive.

Once the spine is fully developed, the epidermis that covered it during its growth disintegrates. However, the outer layer (cortex) of the spine is not directly in contact with seawater. In fact, as soon as the epidermis disappears, a biofilm and numerous epibionts colonize the cortex. They could play a significant role in the protection of the spine in acidified seawater. Analogously, the periostracum of mollusc shells protects these from corroding water (Tunnicliffe et al. 2009; Thomsen et al. 2010). However, epibionts can have various types of attachment: anchoring, molding, cementing, or corroding (David et al. 2009). The last type could have an antagonist effect, actually increasing the surface area of cortex in contact with seawater. Moreover, acidification could have a positive effect on the corroding activity of some epibionts. For instance, bioerosion capacity and boring rates of sponges in corals increase at low pH (Duckworth & Peterson 2013; Wisshak et al. 2012). Nevertheless, corroding epibionts do not appear to be the dominating epibionts on cidaroid spines (David et al. 2009). The proportion of epibionts covering the shaft of the spine varies according to the environment (Hétérier et al. 2004), which should be taken into account when considering their potential protective effects. Furthermore, cidaroids are able to "autotomize" the shaft of their primary spines (Prouho 1887; Cutress 1965; Märkel & Röser 1983b). This process could also account for the long term resilience of cidaroids in undersaturated conditions.

In conclusion, the higher density and the lower magnesium concentration of the cortex relative to that of the underlying stereom seem to be the main factors reducing its dissolution in acidified conditions, at least in the case of spines of the shallow-water species *Phyllacanthus imperialis*. The role of the organic matrix is minor. The presence of a biofilm and epibionts could play an important role in covering the cortex and shielding it from direct contact with seawater. This could mean that symbioses between cidaroids and epibionts could include a mutualistic component beside the "collective parasitism" suggested by David et al. (2009) (David, unpubl. data).

Additional study aiming to determine if the same dissolution-resistant spine properties are found in deep-water cidaroids living under the saturation horizons for calcium carbonates would be worthwhile.

Acknowledgments. The authors thank Bruno David (Université de Bourgogne, France) and an anonymous reviewer for constructive remarks and suggestions. We are grateful to Paul Postiau of Mons University for his assistance with SEM analyses, and to Saloua M'Zoudi and Georges Zaboukis from Brussels University (ULB) for their valuable help. We also thank Prof. Alberto Borges (University of Liège) for providing the Tris and AMP buffers as well as the Center for Applied Technology in Microscopy (Catμ, ULg) for providing access to SEM-EDX analysis facilities. A. Catarino thanks Portugal's "Fundação para a Ciência e a Tecnologia" (FCT) for grant no. SFRH/BM/21387/2005. The study was supported by FRFC contract 2.4532.07.

References

Ameye L, De Becker G, Killian C, Wilt F, Kemps R, Kuypers S, & Dubois P 2001. Proteins and saccharides of the sea urchin organic matrix of mineralization: characterization and localization in the spine skeleton. J. Struct. Biol. 134: 56–66.

Andersson AJ, Mackenzie FT, & Bates NR 2008. Life on the margin: implications of ocean acidification on

Mg-calcite, high latitude and cold-water marine calcifiers. Mar. Ecol. Prog. Ser. 373: 265–273.
Borig P 1933. Über wachstum und regeneration der stacheln einiger seeigle. Z. Morph. Ökol. Tiere 27: 624–653.
Byrne M 2011. Unshelled abalone and corrupted urchins: development of marine calcifiers in a changing ocean. Proc. R. Soc. Lond., Ser. B: Biol. Sci. 278: 2376–2383.
Catarino AI, Guibourt V, Moureaux C, De Ridder C, Compère P, & Dubois P 2013. Antarctic *Ctenocidaris speciosa* spines: lessons from the deep. Cah. Biol. Mar. 54: 649–655.
Cutress BM 1965. Observations on growth in *Eucidaris tribuloides* (Lamarck), with special reference to the origin of the oral primary spines. Bull. Mar. Sci. 5: 797–834.
David B, Choné T, Mooi R, & De Ridder C 2005. Antarctic Echinoidea. Synopses of the Antarctic Benthos, Vol. 10. Koeltz Scientific Books, Königstein. 274 pp.
David B, Stock S, De Carlo F, Hétérier V, & De Ridder C 2009. Microstructures of Antarctic cidaroid spines: diversity of shapes and ectosymbiont attachments. Mar. Biol. 156: 1559–1572.
Del Valls TA & Dickson AG 1998. The pH of buffers based on 2-amino-2- hydroxymethyl-1, 3-propanediol ("TRIS") in synthetic sea water. Deep-Sea Res. 1: 1541–1554.
Doncaster CP & Davey AJ 2007. Analysis of Variance and Covariance. Cambridge University Press, UK. 288 pp.
Dubois P 1991. Morphological evidence of coherent organic material within the stereom of postmetamorphic echinoderms. In: Mechanisms and Phylogeny of Mineralization in Biological Systems. Suga S & Nakahara H, eds., pp. 41–45. Springer-Verlag, Tokyo.
Dubois P & Chen C 1989. Calcification in Echinoderms. In: Echinoderm Studies, Vol. 3. Jangoux M & Lawrence JM, eds., pp. 109–178. Balkema, Amsterdam.
Duckworth AR & Peterson BJ 2013. Effects of seawater temperature and pH on the boring rates of the sponge *Cliona celata* in scallop shells. Mar. Biol. 160, 27–35. doi:10.1007/s00227-012-2053-z.
Dupont S, Dorey N, & Thorndyke M 2010. What meta-analysis can tell us about vulnerability of marine biodiversity to ocean acidification? Estuar. Coast. Shelf Sci. 89: 182–185.
Feely RA, Sabine CL, Lee K, Berelson W, Kleypas J, Fabry VJ, & Millero FJ 2004. Impact of anthropogenic CO_2 on the $CaCO_3$ system in the oceans. Science 305: 362–366.
Feely RA, Doney SC, & Cooley SR 2009. Ocean acidification. Present conditions and future changes in a high-CO_2 world. Oceanography 22: 36–47.
Gran G 1952. Determination of the equivalence point in potentiometric titrages-Part II. Analyst 77: 661–671.
Grossmann JN & Nebelsick JH 2013. Comparative morphological and structural analysis of selected cidaroid and camarodont sea urchin spines. Zoomorphology 132: 301–315.
Harper EM 2000. Are calcitic layers an effective adaptation against shell dissolution in the Bivalvia? J. Zool. 251: 179–186.
Heatfield BM 1971. Growth of the calcareous skeleton during regeneration of spines of the sea urchin, *Strongylocentrotus purpuratus* (Stimpson): a light and scanning electron microscopic study. J. Morphol. 134: 57–90.
Hétérier V, De Ridder C, David B, & Rigaud T 2004. Comparative biodiversity of ectosymbionts in two Antarctic cidarid echinoids, *Ctenocidaris spinosa* and *Rhynchocidaris triplopora*. In: Echinoderms München. Heinzeller T & Nebelsick JH, eds., pp. 201–205. Taylor & Francis, London.
Hofmann GE & Todgham AE 2010. Living in the now: physiological mechanisms to tolerate a rapidly changing environment. Annu. Rev. Physiol. 72: 127–145.
Kroh A & Smith AB 2010. The phylogeny and classification of post-Palaeozoic echinoids. J. Syst. Palaeontol. 8: 147–212.
Märkel K & Röser U 1983a. The spine tissues in the echinoid *Eucidaris tribuloides*. Zoomorphology 103: 25–41.
——— 1983b. Calcite resorption in the spine of the echinoid *Eucidaris tribuloides*. Zoomorphology 103: 43–58.
Märkel K, Kubanek F, & Willgallis A 1971. Polykristalliner Calcit bei Seeigeln (Echinodermata, Echinoidea). Z. Zellforsch 119: 355–377.
Melzner F, Gutowska MA, Langenbuch M, Dupont S, Lucassen M, Thorndyke MC, Bleich M & Pörtner H-O 2009. Physiological basis for high CO_2 tolerance in marine ectothermic animals: pre-adaptation through lifestyle and ontogeny? Biogeosciences 6: 2313–2331.
Millero FJ 2001. Physical Chemistry of Natural Waters. Wiley-Interscience, New-York. 654 pp.
Mischor B 1975. Zur Morphologie und Regeneration der Hohlstacheln von *Diadema antillarium* Philippi und *Echinothrix diadema* (L.) (Echinoidea, Diadematidae). Zoomorphology 82: 243–258.
Morse JW & Mackenzie FT 1990. Geochemistry of Sedimentary Carbonates. Elsevier Science Publishers B.V, Amsterdam. 707 pp.
Morse JW, Andersson AJ, & Mackenzie FT 2006. Initial responses of carbonate-rich shelf sediments to rising atmospheric pCO_2 and "ocean acidification": role of high Mg-calcites. Geochim. Cosmochim. Acta 70: 5814–5830.
Mortensen Th 1928. A monograph of the Echinoidea; I. Cidaroidea, 1- 551. c.A. Reitzel, Kebenhavn; H. Milford, Oxford University Press, London.
Moureaux C, Pérez-Huerta A, Compère P, Zhu W, Leloup T, Cusack M, & Dubois P 2010. Structure, composition and mechanical relations to function in sea urchin spine. J. Struct. Biol. 170: 41–49.
Orr JC, Fabry VJ, Aumont O, Bopp L, Doney SC, Feely RA, Gnanadesikan A, Gruber N, Ishida A, Joos F, Key RM, Lindsay K, Maier-Reimer E, Matear R, Monfray P, Mouchet A, Najjar RG, Plattner G-K, Rodgers KB, Sabine CL, Sarmiento JL, Schlitzer R,

Slater RD, Totterdell IJ, Weirig M-F, Yamanaka Y, & Yool A 2005. Anthropogenic ocean acidification over the twenty-first century and its impact on calcifying organisms. Nature 437: 681–686.

Pelejero C, Calvo E, & Hoegh-Guldberg O 2010. Paleoperspectives on ocean acidification. Trends Ecol. Evol. 35: 332–344.

Pierrot D, Lewis E, & Wallace DWR 2006. MS Excel Program Developed for CO_2 System Calculations. ORNL/CDIAC-105a. Carbon dioxide Information Analysis Center, Oak Ridge National Laboratory, U.S. Department of Energy, Oak Ridge, Tennessee.

Plummer LN & Mackenzie FT 1974. Predicting mineral solubility from rate data: application to the dissolution of Mg- calcites. Am. J. Sci. 274: 61–83.

Politi Y, Arad T, Klein E, Weiner S, & Addadi L 2004. Sea urchin spine calcite forms via a transient amorphous calcium carbonate phase. Science 306: 1161–1164.

Pörtner H 2008. Ecosystem effects of ocean acidification in times of ocean warming: a physiologist's view. Mar. Ecol. Prog. Ser. 373: 203–217.

Pörtner H, Langenbuch M, & Reipschläger A 2004. Biological impact of elevated ocean CO_2 concentrations: lessons from animal physiology and earth history. Oceanography 60: 705–718.

Prouho H 1887. Recherches sur le *Dorocidaris papillata* et quelques autres échinides de la Méditerranée. Arch. Zool. Exp. 5: 214–380.

Schöne BR, Dunca E, Fiebig J, & Pfeiffer M 2005. Mutvei's solution: an ideal agent for resolving microgrowth structures of biogenic carbonates. Palaeogeogr., Palaeoclimatol. Palaeoecology 228: 149–166.

Smith A 1980. Stereome microstructure of the Echinoid test. Spec. Pap. Palaeontol. 25: 1–81.

Stumpp M, Trübenbach K, Brennecke D, Hu MY, & Melzner F 2012. Resource allocation and extracellular acid–base status in the sea urchin *Strongylocentrotus droebachiensis* in response to CO_2 induced seawater acidification. Aquat. Toxicol. 110–111: 194–207.

Thomsen J, Gutowska MA, Saphörster J, Heinemann A, Trübenbach K, Fietzke J, Hiebenthal C, Eisenhauer A, Körtzinger A, Whal M, & Melzner F 2010. Calcifying invertebrates succeed in a naturally CO_2-rich coastal habitat but are threatened by high levels of future acidification. Biogeosciences 7: 3879–3891.

Tunnicliffe V, Davies KTA, Butterfield DA, Embley RW, Rose JM, & Chadwick WW 2009. Survival of mussels in extremely acidic waters on a submarine volcano. Nature Geosci. 2: 344–348.

Twitchett RJ & Oji T 2005. Early Triassic recovery of echinoderms. C. R. Palevol. 4: 531–542.

Walter LM & Morse JW 1984. Magnesian calcite stabilities: a reevaluation. Geochim. Cosmochim. Acta 48: 1059–1069.

Wisshak M, Schönberg CHL, Form A, & Freiwald A 2012. Ocean acidification accelerates reef bioerosion. PLoS ONE 7(9): e45124. doi:10.1371/journal.pone.0045124.

Zeebe RE 2012. History of seawater carbonate chemistry, atmospheric CO_2, and ocean acidification. Annu. Rev. Earth Planet. Sci. 40: 141–165.